Hard diffraction in hadron-hadron interactions and in photoproduction

R. Engel

Universität Leipzig, Fachbereich Physik, D-04109 Leipzig, Germany
and Universität Siegen, Fachbereich Physik, D-57068 Siegen, Germany

J. Ranft

CERN, CH-1211 Genève 23, Switzerland

S. Roesler

Universität Siegen, Fachbereich Physik, D-57068 Siegen, Germany

Hard single diffractive processes are studied within the framework of the triple-Pomeron approximation. Using a Pomeron structure function motivated by Regge theory we obtain parton distribution functions which do not obey the momentum sum rule. Based on Regge factorization, cross sections for hard diffraction are calculated. Furthermore, the model is applied to hard diffractive particle production in photoproduction and in $p\bar{p}$ interactions.

PACS number(s): 13.85.Hd, 11.55.Jy, 12.38.Lg

I. INTRODUCTION

A significant fraction of events in high energy hadron-hadron interactions and in photoproduction is characterized by a rapidity gap between a quasielastically scattered primary hadron and a multiparticle final state. These single diffractive interactions can be understood in terms of Pomeron exchange.

As suggested by Ingelman and Schlein [1] there is now, in addition to the well-investigated soft diffractive particle production, experimental evidence for single diffractive jet production in both $p\bar{p}$ and ep interactions [2–7]. Characteristic features of these jets are very similar to the ones produced in nondiffractive events. This observation suggests that it might be possible to apply models based on perturbative QCD to describe hard diffractive scattering processes between hadrons or photons and Pomerons.

It is useful to distinguish between noncoherent diffraction and processes where the Pomeron enters the hard scattering as a whole. Models based on noncoherent interactions usually assume the Pomeron to be a partonic object, the parton momenta obeying parton distribution functions (PDF's) [1,8–12]. According to the assumptions made, these PDF's strongly differ in the partons considered, in their shapes, and in their normalizations. In addition, one can consider interactions where almost all the Pomeron momentum enters the hard scattering. First signs for a "superhard" Pomeron structure in $p\bar{p}$ interactions were reported by the UA8 Collaboration [3]. These effects may manifest themselves in a breakdown of factorization and would lead to a δ-function-like term in the Pomeron structure function. They can be explained by mechanisms called "coherent hard diffraction" [13] or by means of a direct Pomeron-quark coupling [9,14,15]. However, the experimental information on diffractive interactions containing jets in the final state is still limited

and does not allow one to draw definite conclusions on the Pomeron structure.

In the present paper we discuss hard diffraction in the framework of the two-component dual parton model [16–19]. We use an ansatz developed by Capella *et al.* [20,21] which is based on Regge theory to obtain the Pomeron PDF's. Further assumptions on the normalization of the quark distributions are not necessary since this is given by $F_2^{I\!P}$. Features of particle production in hard diffractive photoproduction and in hard diffractive $p\bar{p}$ interactions are investigated and compared to data [3,5].

The paper is organized as follows. In Sec. II we describe the way hard diffraction is treated in our model. We especially focus on the PDF's of the Pomeron. Using Monte Carlo realizations of the model, we discuss hard diffractive particle production and calculate hard diffractive cross sections in Sec. III. A summary is given in Sec. IV.

II. DESCRIPTION OF THE MODEL

A. The triple-Pomeron approximation

Within Regge theory, high mass single diffractive processes are understood by means of triple-Pomeron exchange (see Fig. 1). Using Reggeon field theory [22] this graph is treated as usual Feynman graph. The Pomerons shown in Fig. 1 are defined by propagators $\xi_{I\!P}(t)(s/s_0)^{\alpha_{I\!P}(t)}$ and cannot be considered as particles [23]. In lowest order the differential diffractive cross section is given by the unitarity cut (Fig. 1)

$$\frac{d^2\sigma_{3I\!P}(s,t)}{dt\,dM^2} = \frac{1}{16\pi s^2}|g_{11'}^{I\!P}(t)|^2 g_{22}^{I\!P}(0)\Gamma^{3I\!P}(t)|\xi_{I\!P}(t)|^2$$
$$\times \left(\frac{s}{M^2}\right)^{2\alpha_{I\!P}(t)}\left(\frac{M^2}{s_0}\right)^{\alpha_{I\!P}(0)}. \qquad (1)$$
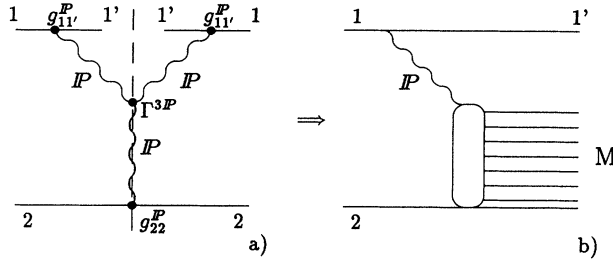
FIG. 1. A cut triple-Pomeron graph (a) describes multi-particle final states characterized by a rapidity gap (b).

With M we denote the mass of the diffractively excited system. $g_{11'}^{I\!P}$, $g_{22}^{I\!P}$, and $\Gamma^{3I\!P}$ are the various couplings as shown in Fig. 1. $\xi_{I\!P}(t)$ is the usual signature factor

$$\xi_{I\!P}(t) = -\frac{1 + e^{-i\pi\alpha_{I\!P}(t)}}{\sin[\pi\alpha_{I\!P}(t)]}.$$ (2)

$\alpha_{I\!P}(t) = 1 + \Delta + \alpha'_{I\!P}(0)t$ is the Pomeron trajectory with the intercept $1 + \Delta$, and $s_0 = 1$ GeV^2. Introducing an effective Pomeron-particle cross section [23]

$$\sigma_{\text{tot}}^{aI\!P}(M^2, t) = g_{22}^{I\!P}(0)\frac{\Gamma^{3I\!P}(t)}{s_0}\left(\frac{M^2}{s_0}\right)^{\alpha_{I\!P}(0)-1},$$ (3)

Eq. (1) can be interpreted as a product of a Pomeron flux factor and this cross section:

$$\frac{d^2\sigma_{3I\!P}(s, t)}{dt\, dM^2} = \frac{1}{16\pi s^2}|g_{11'}^{I\!P}(t)|^2|\xi_{I\!P}(t)|^2$$
$$\times \frac{s^{2\alpha_{I\!P}(t)}}{(M^2)^{2\alpha_{I\!P}(t)-1}}\sigma_{\text{tot}}^{aI\!P}(M^2, t).$$ (4)

To estimate the contribution of hard diffraction (an example of such a process is shown in Fig. 2) to the single diffractive cross section, $\sigma_{\text{tot}}^{aI\!P}$ can be replaced by the hard Pomeron-hadron and/or photon cross section $\sigma_h^{aI\!P}$. We obtain $\sigma_h^{aI\!P}$ applying lowest order perturbative QCD, i.e., in the case of hadron or resolved photon interactions,
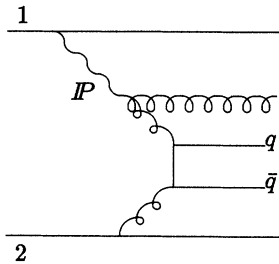

FIG. 2. Example for a hard diffractive scattering process. A gluon of the Pomeron undergoes a hard scattering with a gluon of the lower particle labeled 2.

$$\sigma_h^{aI\!P} = \sum_{i,j,k,l}\frac{1}{1 + \delta_{kl}}\int_0^1 dx_1 \int_0^1 dx_2 \int d\hat{t}\, \frac{d\sigma_{\text{QCD}}^{i,j\to k,l}}{d\hat{t}}$$
$$\times f_a^i(x_1, Q^2)f_{I\!P}^j(x_2, Q^2)\,\Theta(p_\perp - p_\perp^{\text{cutoff}}),$$ (5)

and for direct photon-Pomeron interactions

$$\sigma_{h,\text{dir}}^{\gamma I\!P} = \sum_{j,k,l}\int_0^1 dx \int d\hat{t}\, \frac{d\sigma_{\text{QCD}}^{\gamma,j\to k,l}}{d\hat{t}}\, f_{I\!P}^j(x, Q^2)$$
$$\times \Theta(p_\perp - p_\perp^{\text{cutoff}}).$$ (6)

We sum over all parton configurations and integrate having a lower cutoff in transverse momentum $p_\perp^{\text{cutoff}}$. Here $f_a^i(x, Q^2)$ are the PDF's of the hadron or photon whereas with $f_{I\!P}^j(x, Q^2)$ we introduce distribution functions of partons inside the Pomeron. A detailed discussion of the Pomeron PDF's will be given in the following section.

The free parameters occurring in Eq. (1), such as the proton-Pomeron coupling constant and the intercept of the Pomeron trajectory, are obtained within the two-component dual parton model (DPM) by fits to data on total, elastic, and diffractive cross sections. We refer to [18,19,24,25] for further details.

B. Parton distributions in the Pomeron

As shown in [9,14,12,21] one can derive a Pomeron structure function $F_2^{I\!P}$ by relating it to the total cross section of virtual photon-proton diffractive deep inelastic scattering. Similarly, to the way the proton structure function F_2^p can be related to $\sigma_{\text{tot}}^{\gamma^* p}$ one gets

$$F_2^{I\!P}(x, Q^2, t) = \frac{Q^2}{4\pi^2\alpha_{\text{em}}}\sigma_{\text{tot}}^{\gamma^* I\!P}(M^2, Q^2, t),$$

$$x = \frac{Q^2}{Q^2 + M^2}.$$ (7)

Convoluting $F_2^{I\!P}$ with a Pomeron flux factor, one obtains the structure function of diffractive dissociation. Using Regge factorization it is possible to calculate $F_2^{I\!P}$ from the deuteron structure function F_2^d. The complete formalism is given in Refs. [20,21]. Here we only want to give the main formulas which are necessary to understand the PDF's of the Pomeron we will use afterwards.

The deuteron structure function can be parametrized at moderate values of Q^2 ($Q^2 \leq 5$ GeV^2) [20]:

$$F_2^d(x, Q^2) = S(x, Q^2) + V(x, Q^2)$$

$$= Ax^{-\Delta(Q^2)}(1 - x)^{n(Q^2)+4}\left(\frac{Q^2}{Q^2 + a}\right)^{1+\Delta(Q^2)}$$

$$+ B\, x^{1-\alpha_R}(1 - x)^{n(Q^2)}\left(\frac{Q^2}{Q^2 + b}\right)^{\alpha_R}$$ (8)

with

$$\Delta(Q^2) = \Delta_0 \left(1 + \frac{2Q^2}{Q^2 + d}\right),$$

$$n(Q^2) = \frac{3}{2}\left(1 + \frac{Q^2}{Q^2 + c}\right). \tag{9}$$

We again refer to [20,21] for the exact values of the parameters entering the expressions and a detailed discussion of the Q^2-dependent intercept. The first term in (8) is associated with the Pomeron contribution determining the small-x behavior of sea quarks whereas the second term is parametrized according to secondary Reggeon contributions governing the valence-quark behavior in the deuteron. Furthermore, at low x and moderate photon virtualities Q^2, the ratio between the deuteron- and Pomeron-photon cross sections can be approximated by Regge factorization (see Fig. 3), i.e., is equal to the ratio of the triple-Pomeron and deuteron-Pomeron coupling constants. Thus one can relate the Pomeron structure function $F_2^{I\!P}(x, Q^2, t)$ to the deuteron structure function $F_2^d(x, Q^2)$ by the substitutions

$$F_2^{I\!P}(x, Q^2, t) = F_2^d(x, Q^2; A \to e(t)A, B \to f(t)B,$$
$$\times n(Q^2) \to n(Q^2) - 2). \tag{10}$$

e and f are ratios of coupling constants. The t dependence of the Pomeron PDF is completely given by the ratios e and f, i.e., by the t dependence of the triple-Pomeron coupling. We use $e(0) = 3f(0) = 0.1$ [21] and an exponential dependence of the triple-Pomeron coupling on t with the slope $b = 0.5$ GeV^{-2} [23,19,26]. The substitution $n(Q^2) \to n(Q^2) - 2$, for example, is due to the similarity of the valence-quark distribution in the Pomeron and a meson. Using Eq. (10) and the definition

$$F_2^{I\!P}(x, Q^2, t) = \sum_q e_q^2 x[f_{I\!P}^q(x, Q^2; t) + f_{I\!P}^{\bar q}(x, Q^2; t)] \tag{11}$$

where e_q are the corresponding quark charges, we obtain,
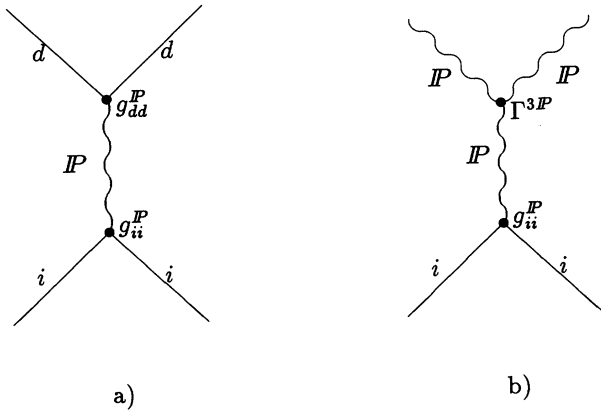

a)   b)

FIG. 3. The diagram in (a) describes elastic i-deuteron scattering and corresponds to the proton structure function if i is a virtual photon. Replacing the deuteron in (a) by a Pomeron, the Regge diagram associated with the Pomeron structure function as shown in (b) is obtained.

at moderate Q^2 values for the Pomeron PDF's,

$$xf_{I\!P}^u(x, Q^2; t) = xf_{I\!P}^{\bar u}(x, Q^2; t)$$
$$= xf_{I\!P}^d(x, Q^2; t)$$
$$= xf_{I\!P}^{\bar d}(x, Q^2; t)$$
$$= \frac{3}{4}e(t)S(x, Q^2) + \frac{9}{10}f(t)V(x, Q^2),$$

$$xf_{I\!P}^s(x, Q^2; t) = xf_{I\!P}^{\bar s}(x, Q^2; t) = \frac{3}{4}e(t)S(x, Q^2). \tag{12}$$

For simplicity, we assume an SU(3)-symmetrical sea of light quarks. The charm-quark distribution of the Pomeron is suppressed at the Q^2 values considered so far. In contrast to the nucleon it is not possible to determine the normalization of the gluon distribution in the Pomeron by the momentum sum rule. We are therefore free to choose a specific form and normalization. With respect to the experimental observations which favor a relatively "hard" structure we use

$$xf_{I\!P}^g(x, Q_0^2; t) = K(Q_0^2, t)x(1 - x), \tag{13}$$

where $K(Q_0^2, t)$ depends on the normalization chosen. In the following we take the normalization of the gluon distribution according to the scaling factor resulting for the quark distribution from Eq. (10):

$$K(Q_0^2, t) = 6e(t)\left(1 - \sum_{q,\bar q}\int_0^1 dx\, xf_d^q(x, Q_0^2)\right). \tag{14}$$

As already mentioned all distributions obtained are limited to $Q^2 \leq 5$ GeV^2. In order to get PDF's of the Pomeron at higher Q^2 values we take (12) and (13) as input distributions for a QCD evolution in the leading logarithmic approximation [12]. The evolution was done using the code of [27,28] with $Q_0^2 = 2$ GeV^2. The result is shown in Figs. 4 and 5, where we have plotted $xf_{I\!P}^u, xf_{I\!P}^s$, and $xf_{I\!P}^g$ for different values of Q^2. Within this formalism, the normalization of the Pomeron PDF's is given by

$$N_q = \sum_{q,\bar q}\int_0^1 dx\, xf_{I\!P}^q(x, Q^2, t),$$

$$N_g = \int_0^1 dx\, xf_{I\!P}^g(x, Q^2, t), \tag{15}$$

which is shown for $t = 0$ GeV^2 in Fig. 6. Note that Regge factorization together with (14) leads to the fact that the Pomeron PDF's do not satisfy the momentum sum rule. The hardness of the u- and d-quark distributions at low values of Q^2 is governed by the valence part of (10), i.e., for $x > 0.5$ we are mainly dealing with a $\sqrt{x}(1 - x)^{n(Q^2)-2}$ behavior, $n(Q^2)$ being about 2.0–3.0 ($c = 3.55$ [20]). We note that this behavior is similar to the Q^2-independent predictions of [9,14], whereas at high Q^2 values our quark distributions become softened due to the sea-quark contribution and the QCD evolution.

Furthermore, we show in Fig. 7 the structure function

$F_2^{I\!P}$ for different Q^2 scales. Again, the flat shape of $F_2^{I\!P}$ is determined by the valence-quark distributions.

III. PARTICLE PRODUCTION IN HARD DIFFRACTIVE INTERACTIONS

A. Sampling of hard single diffractive events

The Monte Carlo treatment of soft single diffractive hadron-hadron interactions within the two-component DPM is described in [17,18]. The generation of single diffractive events in photoproduction will be discussed elsewhere [29]. Here we want to focus on the way the existing models have been extended to diffractive jet production. This has been done for $p\bar{p}$ collisions using an extension to the DTUJET-93 code [30] and for $p\bar{p}$ as well as γp collisions using the DTUJET-PHOJET code [31,29].

The Monte Carlo (MC) implementation is similar to that of the usual hard scattering processes (i.e., processes involving high p_t) between hadrons or between hadrons and photons. The main differences are that (i) the interaction is boosted to the rest system of the diffractively excited "blob," and the c.m. energy is therefore given by the diffractive mass, and (ii) one hadron is replaced by a Pomeron with a virtuality t. The momenta of the partons entering the hard $2 \longrightarrow 2$ scattering process are obtained using conventional PDF's of hadrons and photons [32–34] and the PDF's of the Pomeron introduced in the previous section. Initial state radiation which significantly modifies the multiparticle final state of interactions involving high transverse momenta has been included. The chain system to be hadronized using JETSET 7.3 [35,36] is determined by the color flow, taking cross sections for different color flow diagrams into consideration [37,38].

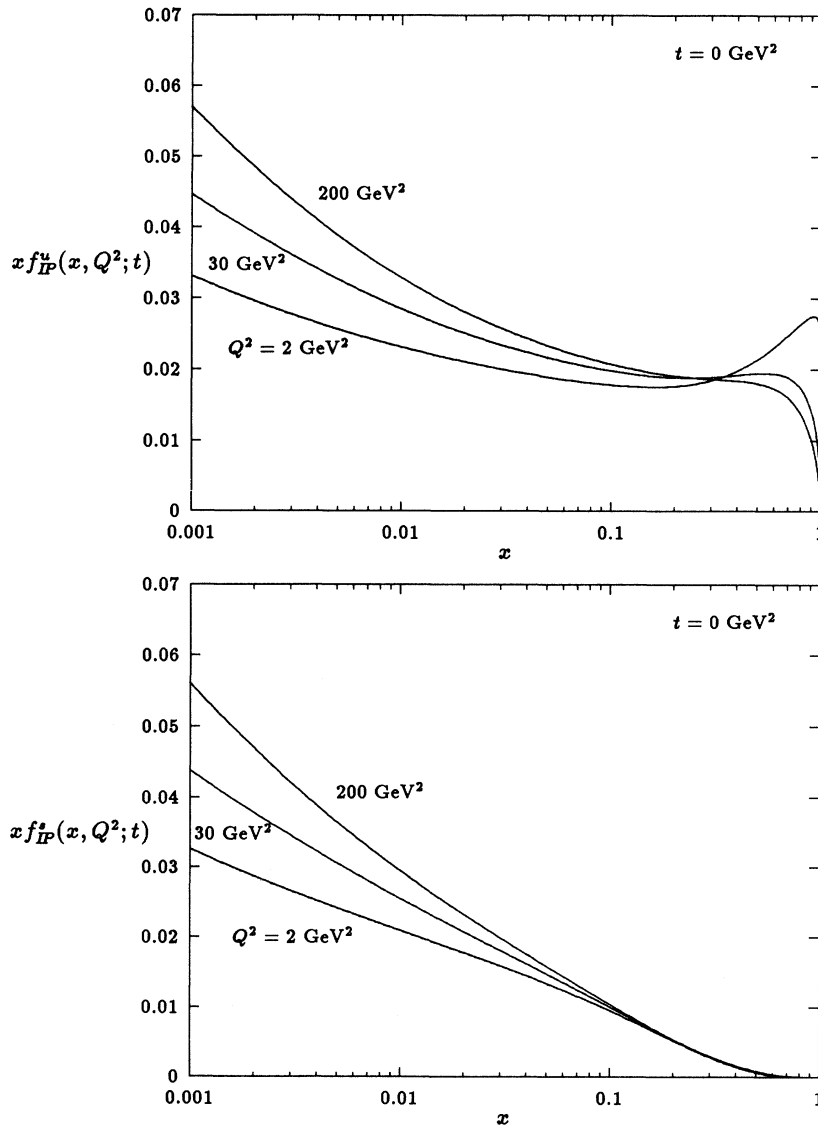Parts of the MC realization of hard diffraction are tech-

FIG. 4. u- and s-quark distributions in the Pomeron are plotted for different values of Q^2. The initial distribution of the QCD evolution is shown for $Q_0^2 = 2$ GeV^2.

nically similar to the ones described in [39,40], which were so far mainly used to understand the underlying interactions. However, we would like to emphasize that our starting points are completely different. Our investigation is based on the two-component DPM which treats soft and hard scattering processes in a unified manner. The free parameters are fixed by fits to cross section data. Similarly to [39,40] we assume hard diffraction to be based on a partonic structure of the Pomeron but we start from a Pomeron structure function which is determined by fits to data on the proton structure function and a ratio of coupling constants which follows from the model. There is no further freedom in choosing a specific x and Q^2 dependence of the quark distribution inside the Pomeron. The normalizations of the Pomeron PDF's (and therefore the hard diffractive cross sections) are obtained from the model rather than imposing additional assumptions [39,40].

B. Hard diffraction in photoproduction

Recent measurements at the electron proton collider HERA at DESY have shown that a substantial part of
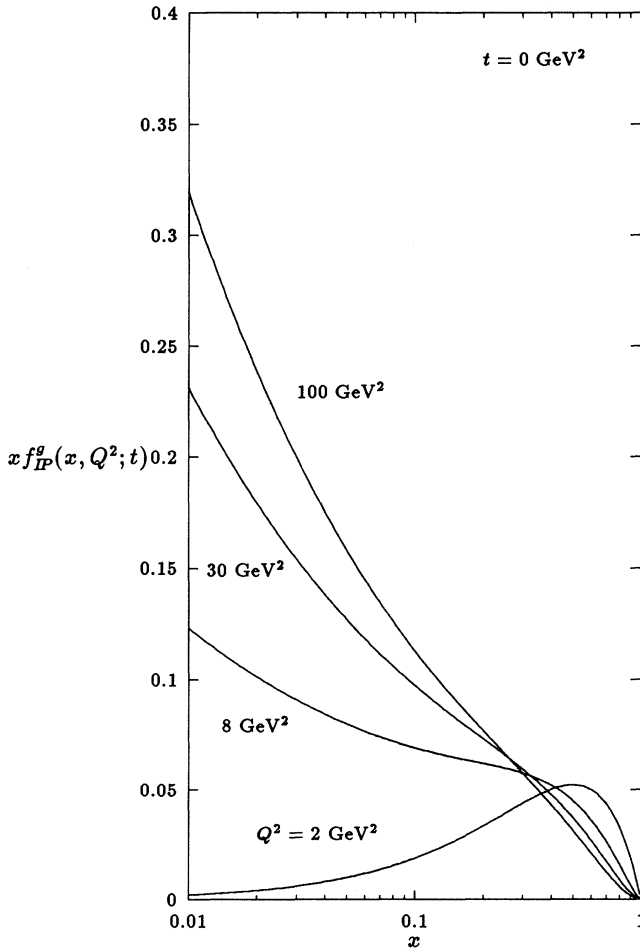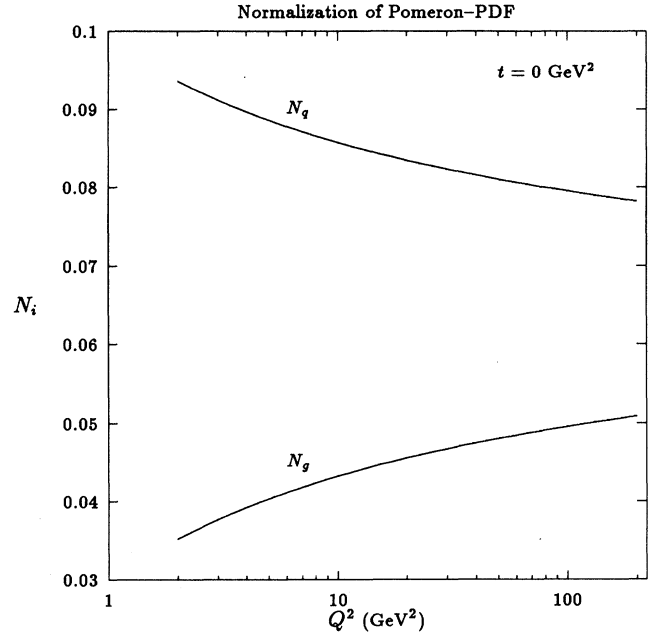

FIG. 6. Normalization of the quark and gluon distribution functions of the Pomeron.

minimum bias photoproduction [5,7] and deep inelastic scattering [4,6] events exhibits diffractive features similar to hadron-hadron scattering. The first distributions of so called rapidity gap events have been published [5,7], but the data are not yet corrected for acceptance and do not allow absolute comparisons. We will apply the model developed to investigate diffraction dissociation of photons in quasireal photon-hadron scattering and we understand that more data will be published soon.

The simulation of diffractive events in photoproduction can be done as for diffraction in hadron-hadron scattering, substituting the hadron-Pomeron scattering subprocess by photon-Pomeron scattering. In the calculation of
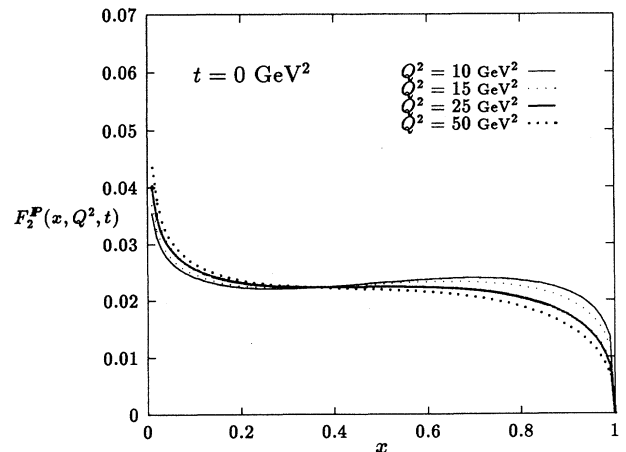

FIG. 5. Gluon distribution in the Pomeron shown for different values of Q^2.

FIG. 7. Pomeron structure function $F_2^{I\!P}(x, Q^2; t = 0)$.

the total diffractive cross section, the absorptive corrections due to multiple photon-hadron scattering are taken into account [19]. For the simulation of photon-Pomeron scattering we neglect unitarity corrections (e.g., multiple photon-Pomeron scattering) which become important only for very high diffractive masses.[1] Thus the simulation of hard photon-Pomeron scattering follows directly from Eqs. (5) and (6). The Pomeron flux is calculated using Eq. (1).

To calculate ep photoproduction cross sections, the flux of quasireal photons has to be estimated. Here we apply the improved Weizsäcker-Williams approximation [41]

$$f_{e/\gamma}(y) = \frac{\alpha}{2\pi} \left(\frac{1 + (1+y)^2}{y} \ln \frac{Q^2_{\max}}{Q^2_{\min}} - \frac{1(1-y)}{y} \right) \quad (16)$$

with the kinematical cuts

$$0.25 < y < 0.7, \qquad Q^2_{\min} = 3 \times 10^{-8} \text{ GeV}^2,$$

$$Q^2_{\max} = 10^{-2} \text{ GeV}^2. \quad (17)$$

y and Q^2 denote the energy fraction taken by the photon from the electron and the photon virtuality, respectively.

Using our Monte Carlo program, complete hadronic final states have been generated and analyzed. According to the experimental conditions only events passing the $\eta_{\max}$ cut [42,6] have been accepted for further analysis. In addition, a few less restrictive cuts have been applied to match the experimental selection procedure described in [5].

In Fig. 8 we show the transverse momentum distribution of charged particles for the selected rapidity gap events in the pseudorapidity range $-1.5 < \eta_{\text{lab}} < 1.5$. The absolute cross sections obtained with the model are given. Together with the predictions we show uncorrected data of the H1 Collaboration [5] on charged tracks. It is expected that the shape of this distribution can be compared with calculations for transverse momenta higher than 1 GeV/c [43]. Note that the data are scaled in order to compare their shape to our calculation. The systematic difference between the model and the calculation at low $p_\perp$ can be qualitatively explained by the $p_\perp$-dependent experimental acceptance in this region [43]. In addition, the contribution from direct photon processes is shown.

Using a cone jet algorithm similar to the one used in [5] the transverse energy and pseudorapidity distributions of jets with $E_t > 4$ GeV are calculated. In Fig. 9 we show the transverse energy distribution of jets together with uncorrected H1 data [5]. Since the so-called jet pedestal is small in diffractive events [5,7,44] the transverse jet distribution should not be drastically influenced by acceptance effects. In Fig. 10 the corresponding pseudorapidity distribution of jets is compared to H1 data. In

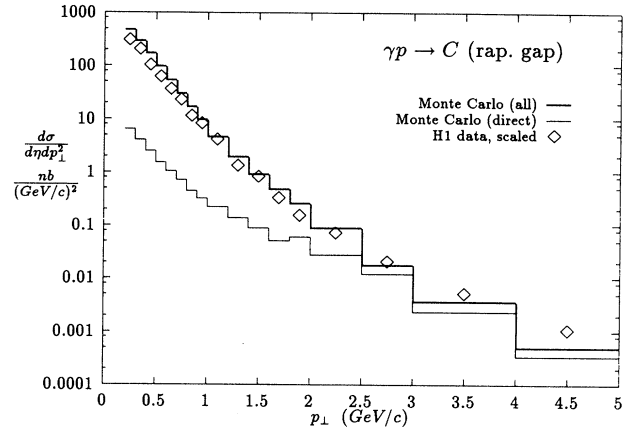[1] High diffractive masses are suppressed by applying the experimental cuts.

FIG. 8. Inclusive charged particle cross section for particle with $|\eta_{\text{lab}}| < 1.5$. The model predictions are shown as full lines and compared to H1 data (see text).

both figures, the H1 data are again scaled to compare their shape with the model predictions.

C. Hard diffractive proton-antiproton interactions

1. Cross sections for hard single diffraction

An estimation of cross sections for hard diffractive events containing jets in the final state can be obtained using Regge factorization [Eq. (4)] together with the hard Pomeron-particle cross sections given in Eqs. (5) and (6). However, the cross sections depend strongly on the partonic cutoff in transverse momentum which enters the integrations. In addition, further uncertainties arise from
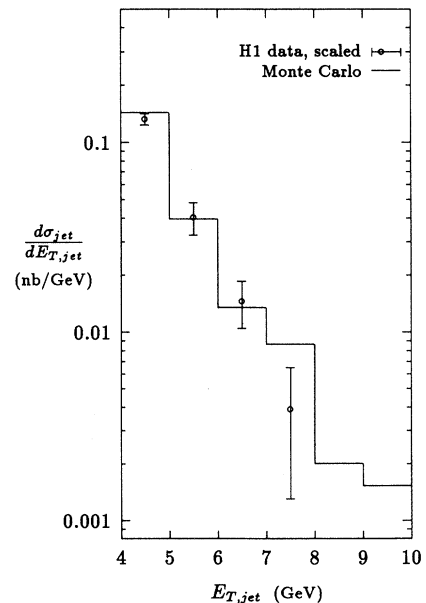

FIG. 9. Inclusive transverse energy distribution of jets calculated for jets with $|\eta_{\text{jet}}| < 1.5$ and compared to H1 data.
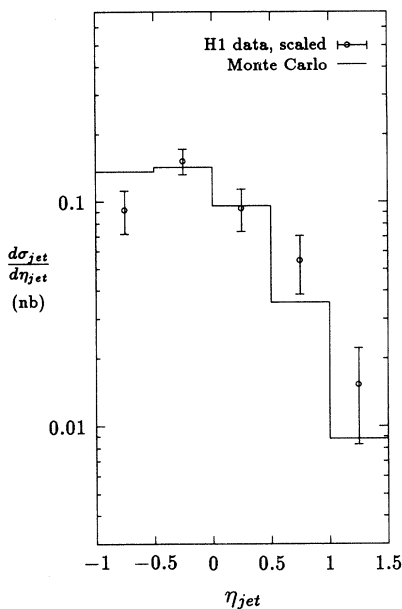
FIG. 10. Inclusive pseudorapidity distribution of jets in rapidity gap events with $E_{t,\text{jet}} > 4$ GeV calculated with the model and shown with H1 data.

choosing a certain scale in (5) and (6) and from the definition of a diffractive event itself, i.e., from the t and M^2 ranges the differential hard diffractive cross section has to be integrated over.

Reliable predictions for cross sections in hard diffraction can therefore only be given for a certain experimental setup taking into account all kinematical cuts applied and jet rates based on jet-finding algorithms which were used to obtain the experimental results. This has been done for the experimental setup of the UA8 Collaboration [3] with a jet-finding algorithm which will be described further below. We calculate the ratio of the hard diffractive cross section and the total diffractive cross section using
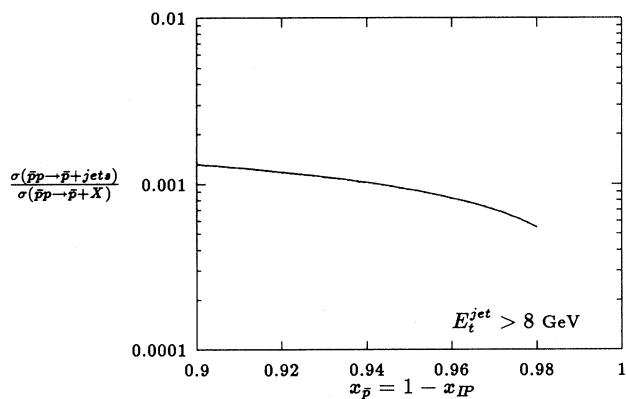

FIG. 11. Ratio of hard diffractive cross sections for two-jet events and total diffractive cross sections. According to forthcoming UA8 data [47,46] to which our calculation might be compared, a lower cut in transverse energy of 8 GeV has been applied.

the Martin-Roberts-Stirling set D0' (MRS D0') [32] set for the parton distributions in the proton (or antiproton) and the t-dependent proton-Pomeron coupling $g_{p\!I\!P}(t) = g_{p\!I\!P}(0) \exp(b_0 t)$, its value at $t = 0$ $g_{p\!I\!P}(0) = 6.2$ $\sqrt{\text{mb}}$ and the slope $b_0 = 1.6$ GeV^{-2}, $\Gamma^{3\!I\!P}(t = 0) = 0.08$ $\sqrt{\text{mb}}$ GeV^2, $\Delta = 0.078$, $\alpha'(0) = 0.25$ GeV^{-2}, and $Q^2 = p_\perp^2$ [19]. To obtain ratios which correspond to the UA8 cuts we multiply these values by the fraction of those events which contain at least two jets of a transverse energy $E_t^{\text{jet}} \geq E_t^{\text{cutoff}}$ and of a pseudorapidity $|\eta| < 2$ in their final state. Experimental data for these ratios in preliminary form were given in [45]; final values will be available soon [46] and we understand that our calculations shown in Fig. 11 will be consistent with these data [47].

2. Hard diffractive particle production

Hard diffractive proton-antiproton interactions were recently investigated by the UA8 Collaboration [3] at a c.m. energy of 630 GeV. Only limited information on absolute hard diffractive cross sections is available so far [45] (see previous section). It is therefore not possible to compare our model directly to these data. However, since our model is able to describe data on hard diffraction in photoproduction rather well it might be worthwhile to show also predictions for hard diffractive $p\bar{p}$ interactions. In particular we apply the same cuts to the final state as were used in the experiments [3]. This means that the momentum transfer t is limited to values between -1 GeV^2 and -2 GeV^2. Though $|t|$ is rather large the range of diffractive masses M taken into account (126 GeV$\leq M \leq$ 200 GeV) ensures that the Regge limit $s \gg M^2 \gg |t|$ is still satisfied. Jets are identified using a cone algorithm in the η-ϕ plane, with ϕ being the azimuthal angle and $|\eta| < 2$. If a jet with $E_t > 8$ GeV is found the search for its axis is iterated calculating E_t-weighted sums over cells within a unit-cone radius. According to the UA8 data all distributions discussed in this section are normalized to unit area. Our results are obtained with the PDF set MRS D0' for the parton distributions in the proton or antiproton.

As mentioned in [3] a variable sensitive to the partonic structure of the Pomeron could be x_{jet}. It is defined as the longitudinal momentum component of a jet normalized to its maximum value in the Pomeron-antiproton c.m. system. In Fig. 12 we present predictions of our model for momentum fractions of the quasielastically scattered proton x_p between 0.92 and 0.94. As stated by the UA8 Collaboration [3] the data were obtained with essentially full acceptance at positive x_{jet} values; i.e., it can be expected that our calculations agree well with the data also after the corrections have been applied.

In Fig. 13 we show the distribution of the jet pseudorapidity in the antiproton-proton c.m. system again for the same x_p bin. The tail at positive η values is influenced mainly by the structure of the Pomeron.

A variable which may indicate whether there is a "superhard" Pomeron structure is $x_{2\,\text{jets}}$, the longitudinal momentum of a two-jet system, again normalized to its maximum value in the Pomeron-antiproton system. The
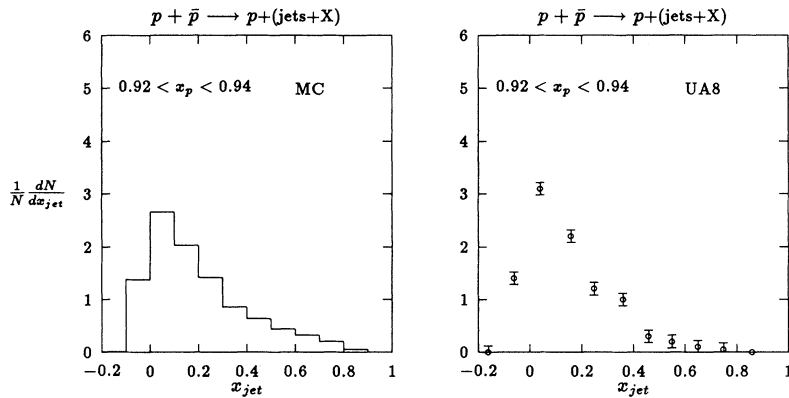
FIG. 12. Distribution of the longitudinal momenta of jets normalized to their maximum value in the c.m. system of the Pomeron-proton interaction. The predictions of the model (labeled "MC") are shown for a momentum fraction of the quasielastically scattered proton between 0.92 and 0.94. The uncorrected UA8 data [3] are plotted separately (labeled "UA8").

results of our calculation are plotted in Fig. 14 showing the contribution from quarks and gluons of the Pomeron PDF separately. Because of the shape of the valence-quark distribution (see Sec. II B) the quarks mainly contribute to higher values of $x_{2\ jets}$ whereas the gluon contribution is peaked around 0.2. Using our Pomeron PDF we therefore obtain a significant fraction of events containing two-jet systems with $x_{2\ jets} > 0.7$. Considering the reasonable agreement found with the γp data the question to what extent a "superhard" contribution is still necessary within our model cannot be answered before corrected measurements are available.

IV. SUMMARY AND CONCLUSIONS

Hard diffraction in hadron-hadron collisions and in photoproduction has been investigated in the framework

of the two-component DPM. Since soft diffractive interactions at collider energies are well described in terms of Pomeron exchange processes, diffractive jet production may provide new information on the Pomeron structure [1].

In the present paper we study features of hard diffractive particle production treating the Pomeron as a partonic object. PDF's of the Pomeron[2] are obtained from a Pomeron structure function motivated by Regge theory. Whereas the quark distributions follow directly from the parametrization of the Pomeron structure function, it is possible to choose an ansatz for the gluon distribution which accounts for the experimentally observed hard Pomeron structure. The normalizations of the quark distributions of the Pomeron are determined by the scaling factor relating the Pomeron structure function to the deuteron structure function. The gluon distribution is assumed to scale with the same factor. Therefore it follows that within our model the momentum sum rule does not
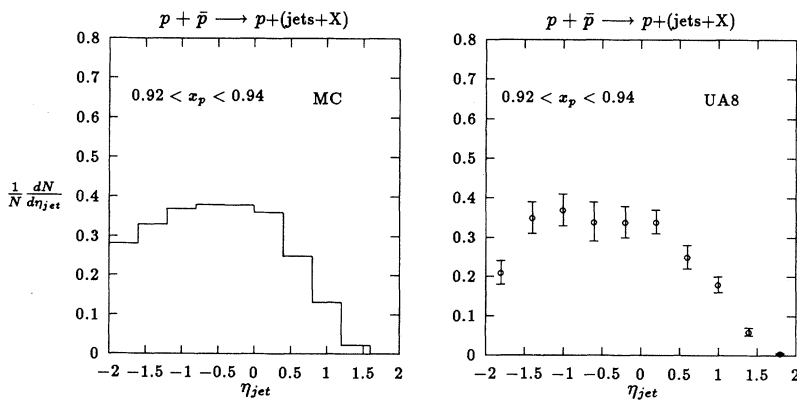

FIG. 13. Pseudorapidity distributions of jets in the c.m. system of the proton-antiproton interaction. The Monte Carlo results (MC) are shown for a momentum fraction of the quasielastically scattered proton between 0.92 and 0.94. The uncorrected UA8 data [3] are plotted separately.

---

[2]The code is available on request from the authors (electronic address: sroesler@cernvm.cern.ch).

$p + \bar{p} \longrightarrow p + (2 \; jets+X)$

MC, all ——
MC, gluon ——
MC, quark · · · ·

$0.90 < x_p < 0.96$

$\frac{1}{N}\frac{dN}{dx_{2\;jets}}$

$x_{2\;jets}$

$p + \bar{p} \longrightarrow p + (2 \; jets+X)$

UA8

$0.90 < x_p < 0.96$

$\frac{1}{N}\frac{dN}{dx_{2\;jets}}$
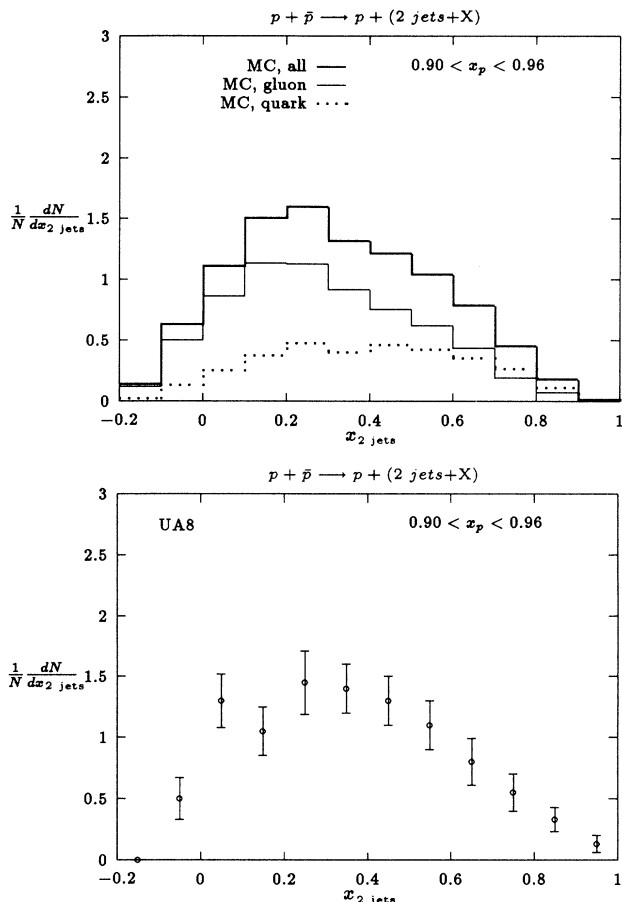
$x_{2\;jets}$

FIG. 14. Distributions of the total longitudinal momentum of a two-jet system normalized to the maximum value for the quark and gluon contribution of the Pomeron and both contributions together are shown. Separately we plot the uncorrected UA8 data [3].

apply for the Pomeron, which is in agreement with the conclusions of [9,10]. The Pomeron PDF's are evolved to high values of Q^2 by applying leading logarithmic QCD evolution equations. Using the triple-Pomeron approxi-

mation, we are able to give predictions on absolute cross sections and distributions.

Cross sections for hard diffraction depend strongly on kinematical cuts and on assumptions defining an event as being produced diffractively. Predictions can therefore only be given taking a specific experimental setup into account.

We demonstrate that the model and the Pomeron PDF's used are in reasonable agreement with presently available data on hard diffraction in γp collisions from the HERA collider. Since there are no absolute distributions published the comparison was restricted to the shape.

A comparison of hard diffractive particle production in hadron-hadron interactions to data is presently limited to data published by the UA8 Collaboration which do not allow absolute comparisons. Nevertheless, the results obtained within our model look promising and may explain the main features of these processes. We are not yet able to draw any conclusions concerning a possible "superhard" Pomeron structure. Further investigations will be necessary as soon as more data become available. For example, the comparison of the model with data on diffractive heavy flavor production at Fermilab Tevatron should allow to reduce the uncertainties of the gluon distribution in the Pomeron [39].

ACKNOWLEDGMENTS

[1] G. Ingelman and P. E. Schlein, Phys. Lett. **152B**, 256 (1985).

[2] UA8 Collaboration, R. Bonino et al., Phys. Lett. B **211**, 239 (1988).

[3] UA8 Collaboration, A. Brandt et al., Phys. Lett. B **297**, 417 (1992).

[4] H1 Collaboration, T. Ahmed et al., Nucl. Phys. **B429**, 477 (1994).

[5] H1 Collaboration, T. Ahmed et al., Nucl. Phys. **B435**, 3 (1995).

[6] ZEUS Collaboration, M. Derrick et al., Phys. Lett. B **315**, 481 (1993).

[7] ZEUS Collaboration, M. Derrick et al., Phys. Lett. B **346**, 399 (1995).

[8] E. L. Berger, J. C. Collins, D. E. Soper, and G. Sterman, Nucl. Phys. **B286**, 704 (1987).

[9] A. Donnachie and P. V. Landshoff, Phys. Lett. B **191**, 309 (1987).

[10] A. Donnachie and P. V. Landshoff, Nucl. Phys. **B303**, 634 (1988).

[11] G. Ingelman and K. Prytz, Z. Phys. C **58**, 285 (1993).

[12] N. N. Nikolaev and B. G. Zakharov, Z. Phys. C **53**, 331 (1992).

[13] J. Collins, L. Frankfurt, and M. Strikman, Phys. Lett. B **307**, 161 (1993).

[14] A. Donnachie and P. V. Landshoff, Nucl. Phys. **B244**, 322 (1984).

[15] B. Kniehl, H.-G. Kohrs, and G. Kramer, Z. Phys. C **65**, 657 (1995).

[16] A. Capella, U. Sukhatme, C. I. Tan, and J. Tran Thanh Van, Phys. Rep. **236**, 227 (1994).

[17] P. Aurenche et al., Phys. Rev. D **45**, 92 (1992).

[18] S. Roesler, R. Engel, and J. Ranft, Z. Phys. C **59**, 481 (1993).

[19] R. Engel, Z. Phys. C **66**, 203 (1995).

[20] A. Capella, A. Kaidalov, C. Merino, and J. Tran Thanh Van, Phys. Lett. B **337**, 358 (1994).

[21] A. Capella, A. Kaidalov, C. Merino, and J. Tran Thanh Van, Phys. Lett. B **343**, 403 (1995).

[22] M. Baker and K. A. Ter-Martirosyan, Phys. Rep. **28C**, 1 (1976).

[23] A. B. Kaidalov, Phys. Rep. **50**, 157 (1979).

[24] F. W. Bopp, R. Engel, D. Pertermann, and J. Ranft, Phys. Rev. D **49**, 3236 (1994).

[25] R. Engel, F. W. Bopp, D. Pertermann, and J. Ranft, Phys. Rev. D **46**, 5192 (1992).

[26] A. Capella, J. Tran Thanh Van, and J. Kaplan, Nucl. Phys. **B97**, 493 (1975).

[27] A. Devoto, D. W. Duke, and J. F. Owens, Phys. Rev. D **27**, 508 (1983).

[28] P. Aurenche et al., Phys. Lett. B **233**, 517 (1989).

[29] R. Engel (in preparation).

[30] F. W. Bopp et al., Comput. Phys. Commun. **83**, 107 (1994).

[31] R. Engel, in Proceedings of the XXIXth Rencontre de Moriond, Meribel, France, 1994, edited by J. Tran Thanh Van (Editions Frontières, Gif-sur-Yvette, France, 1994), p. 321.

[32] A. D. Martin, R. G. Roberts, and W. J. Stirling, Phys. Lett. B **306**, 145 (1993).

[33] M. Glück, E. Reya, and A. Vogt, Phys. Rev. D **46**, 1973 (1992).

[34] H. Plothow-Besch, Comput. Phys. Commun. **75**, 396 (1993).

[35] T. Sjöstrand, Comput. Phys. Commun. **39**, 347 (1986).

[36] T. Sjöstrand and M. Bengtsson, Comput. Phys. Commun. **43**, 367 (1987).

[37] B. L. Combridge, J. Kripfganz, and J. Ranft, Phys. Lett. **70B**, 234 (1977).

[38] H. U. Bengtsson, Comput. Phys. Commun. **31**, 323 (1984).

[39] P. Bruni and G. Ingelman, in Proceedings of International European Conference on High Energy Physics, Marseille, France, 1993, edited by J. Carr and M. Perrottet (Editions Frontières, Gif-sur-Yvette, France, 1994), p. 595.

[40] H. Jung, Comput. Phys. Commun. **86**, 147 (1995).

[41] S. Frixione, M. Mangano, P. Nanson, and G. Ridolfi, Phys. Lett. B **319**, 339 (1993).

[42] H1 Collaboration, T. Ahmed et al., Phys. Lett. B **299**, 374 (1993).

[43] A. Rostovtsev (private communication).

[44] P. E. Schlein, Talk given at the 14th Meeting of the Large Hadron Collider Committee, CERN, 1994 (unpublished).

[45] P. E. Schlein, in Proceedings of International European Conference on High Energy Physics [39], p. 592.

[46] UA8 Collaboration, A. Brandt et al. (in preparation).

[47] P. E. Schlein (private communication).